Brain Topogr (2017) 30:502–520
DOI 10.1007/s10548-017-0565-z

ORIGINAL PAPER

EEG Microstate Correlates of Fluid Intelligence and Response to Cognitive Training

Emiliano Santarnecchi[1,2,3] · Arjun R. Khanna[1] · Christian S. Musaeus[1,4] · Christopher S. Y. Benwell[1,5] · Paula Davila[1] · Faranak Farzan[6] · Santosh Matham[7] · Alvaro Pascual-Leone[1,8] · Mouhsin M. Shafi[1] · on behalf of Honeywell SHARP Team authors

Received: 30 August 2016 / Accepted: 24 April 2017 / Published online: 10 May 2017

Abstract The neurobiological correlates of human fluid intelligence (Gf) remain elusive. Here, we demonstrate that spatiotemporal dynamics of EEG activity correlate with baseline measures of Gf and with its modulation by cognitive training. EEG dynamics were assessed in 74 healthy participants by examination of fast-changing, recurring, topographically-defined electric patterns termed "microstates", which characterize the electrophysiological activity of distributed cortical networks. We find that the frequency of appearance of specific brain topographies, spatially associated with visual (microstate B) and executive control (microstate C) networks, respectively, is inversely related to Gf scores. Moreover, changes in Gf scores with cognitive training are inversely correlated with changes in microstate properties, indicating that the changes in brain network dynamics are behaviorally relevant. Finally, we find that cognitive training that increases Gf scores results in a posterior shift in the topography of microstate C. These results highlight the role of fast-changing brain electrical states in individual variability in Gf and in the response to cognitive training.

Keywords Fluid intelligence · Abstract reasoning · Microstates · EEG · Cognitive training

Introduction

The characterization of intelligence and elucidation of its neurobiological basis is one of the most intriguing issues in modern psychology and neuroscience (Colom et al. 2010;

Emiliano Santarnecchi and Arjun R. Khanna contributed equally to this work.

Electronic supplementary material The online version of this article (doi:10.1007/s10548-017-0565-z) contains supplementary material, which is available to authorized users.

✉ Mouhsin M. Shafi
mouhsin.shafi@gmail.com

1 Berenson-Allen Center for Non-Invasive Brain Stimulation, Division of Cognitive Neurology, Beth Israel Medical Center, Harvard Medical School, 330 Brookline Ave, West/Baker 5, Boston, MA 02215, USA

2 Siena-Brain Investigation & Neuromodulation Lab (SiBIN), Department of Medicine, Surgery and Neuroscience, Neurology and Clinical Neurophysiology Section, University of Siena, Siena, Italy

3 Siena Robotics and Systems Lab (SIRS-Lab), Engineering and Mathematics Department, University of Siena, Siena, Italy

4 Department of Neurology, Danish Dementia Research Centre (DDRC), Rigshospitalet, University of Copenhagen, Copenhagen, Denmark

5 Centre for Cognitive Neuroimaging, Institute of Neuroscience & Psychology, University of Glasgow, Glasgow, UK

6 Temerty Centre for Therapeutic Brain Intervention, Centre for Addiction and Mental Health, University of Toronto, Toronto, Canada

7 Honeywell Labs, Honeywell Aerospace, Redmond, WA, USA

8 Institut Universitari de Neurorehabilitacio Guttmann, Badalona, Barcelona, Spain

da Rocha et al. 2011; Deary et al. 2010; Neubauer and Fink 2009). The concept of intelligence includes two separate, yet highly correlated components (Gray et al. 2003; Gray and Thompson 2004a): (i) a knowledge-based component, referring to abilities acquired through various forms of education and experience and commonly termed "crystallized intelligence" (Gc); and (ii) a core of knowledge- and language-unrelated functions tightly related to the ability for problem solving and abstract reasoning, termed "fluid intelligence" (G*f*). While G*c* relates to problems requiring the retrieval and organization of previously acquired knowledge, G*f* involves abilities related to abstract thinking, logical and probabilistic reasoning, and other cognitive functions believed to depend on neurophysiological factors that optimize information processing capacity (Gray et al. 2003). Moreover, G*f* is a crucial element in the prediction of socioeconomic factors including academic achievement, cardiovascular disease and longevity (Deary 2008). It also usually declines with age and in many neurodegenerative disorders, and plays a key role in the dramatic functional impairment of many chronic-degenerative neurological conditions (Alexander et al. 1997; Matsuda and Saito 1998; Whalley et al. 2004). Consequently, the characterization of the neurobiological underpinnings of G*f* is of great interest in modern neuroscience, and has relevance for our understanding of general human cognitive function, the effects of education and aging, individual cognitive reserve and functional resilience to neurologic and psychiatric diseases (Santarnecchi et al. 2015b; Stern 2009), and could enable the development of new approaches for cognitive enhancement and rehabilitation (Deary 2008; Haier 2014).

A vast literature on the structural and functional correlates of intelligence have converged on a model emphasizing that reasoning processes involve integration of multiple distributed brain regions into large-scale networks that involve a variety of brain regions, responsible for different cognitive functions encompassing perception and early processing of visual and auditory information, abstract reasoning and elaboration of input, solution generation and testing, optimization, and suppression of competing responses (Jung and Haier 2007). However, the role of different brain networks during early and late processing stages of G*f*-related problem solving is still unclear. Different models stress different contributions for visual, parietal, and prefrontal regions in terms of timing, nature (inhibitory/excitatory), and overall importance of their activations (Colom et al. 2006, 2010; Haier et al. 2004; Jung and Haier 2007; Yuan et al. 2012). For example, one hypothesis suggests that increased efficiency at lower levels of processing (e.g. visual and perceptual stages, loading on occipital and parietal cortices) might be the key to induce a functional cascade of effects towards high-level prefrontal computations (Brumback et al. 2004; Buschman et al. 2011; Melnick et al. 2013; Soulieres et al. 2009). Another model argues that core prefrontal regions related to cognitive control are responsible for the bulk of processing, and therefore play the most relevant role in explaining G*f* variability (Gazzaley et al. 2007; Gong et al. 2005; Kievit et al. 2014; Raz et al. 2008). Intermediate scenarios have also been proposed, postulating equal contributions by prefrontal, posterior-temporal and visual cortices (Narr et al. 2007). Interestingly, a parallel controversy applies to different tasks used to measure G*f*, each of which seek to test "abstract reasoning" but do so by stressing putative G*f* subcomponents (e.g. filtering, working memory, mental rotation) which in turn load on different brain regions (Burgess et al. 2011; Gazzaley et al. 2005). Further studies are needed to parse out the dynamic activity of individual brain regions or networks, and thereby help clarify the relative contribution of different brain regions to G*f*.

Most studies on the neurobiology of intelligence have used correlational approaches examining structural and functional brain properties co-varying with G*f* (or G*c*), such as local and global brain volumes (Jung and Haier 2007; Rushton and Ankney 2009), cortical thickness (Goh et al. 2011), or structural wiring (Chiang et al. 2008), and have consequently modeled G*f* as a static feature dependent on these properties. However, recent studies implementing cognitive training (Au et al. 2014; Jaeggi et al. 2008) or transcranial electrical stimulation (Pahor and Jausovec 2014; Santarnecchi et al. 2013, 2016a) demonstrate the possibility of enhancing G*f* in healthy individuals, and challenge the notion of G*f* as a static and immutable individual feature. These reports also indicate that there is a highly dynamic neurophysiological component of G*f* that ought to be amenable to evaluation using current technologies (Kundu et al. 2013; Langer et al. 2013; Wartenburger et al. 2009). We hypothesized that the degree of convergence between behavioral and neurophysiologic patterns observed before and after interventions that improve G*f* would provide insight into core neurobiological substrates of G*f*, beyond what is achievable by correlational studies involving only single, cross-sectional observations of G*f*.

Given the distribution of interconnected cortical regions that are postulated to give rise to intelligence, neuroimaging techniques capable of detecting the activity of spontaneous large-scale networks hold potential for capturing the complex nature of G*f* (Choi et al. 2008). To this end, fMRI studies suggest that the connectivity, efficiency and other features of so-called "resting-state networks," or RSNs (Damoiseaux et al. 2006), are correlated with intellectual performance (Cole et al. 2012; Santarnecchi et al. 2014, 2015b; Stern 2002; van den Heuvel et al. 2009). However, while fMRI offers valuable insights into the spatial localization of G*f*-related processes, it provides limited information about temporal dynamics. In contrast,

electroencephalography (EEG) can measure cortical electrophysiology at native timescales, and spatiotemporal methods of multichannel EEG signal analysis allow for the study of large-scale distributed networks. One such method is EEG microstate analysis, in which transient (on the order of milliseconds), recurring patterns of electrical activity topographically distributed over the entire electrode array, termed "microstates," are identified and used to parse the multichannel EEG signal into a sequence of alternating brain states (Lehmann 1971). This procedure offers a rich microstate repertoire that can be correlated with many cognitive and functional brain states, including increasing age (Koenig et al. 2002), neuropsychiatric disease (Lehmann et al. 2005; Tomescu et al. 2014), task performance (Koenig et al. 1998; Koenig and Lehmann 1996), drug effects (Michel and Lehmann 1993), and others (Khanna et al. 2015). Recent concurrent EEG-fMRI studies have suggested that EEG microstates and fMRI RSNs arise from the same underlying signal generators (Britz et al. 2010a; Van De Ville et al. 2010), indicating that EEG microstate analysis captures the activity of distributed cortical networks. Indeed, temporal correlation between the appearance of certain microstate classes and resting-state BOLD signal fluctuations have suggested that distinct microstate classes are associated with resting-state networks ascribed to phonological processing, visual imagery, attention reorientation, and subjective interoceptive-autonomic processing (Britz et al. 2010a, b).

In this study, we map the electrophysiological correlates of G*f* by means of EEG microstate analysis (Khanna et al. 2014; Lehmann 1971). We specifically focused on (i) identifying baseline neurophysiologic correlates of G*f* and (ii) verifying that changes in G*f* as a result of an external intervention (a cognitive training program) are associated with changes in the same neurophysiological metrics identified as baseline correlates of G*f*. We hypothesized that features of specific EEG microstates related to the activity of prefrontal/cognitive control (microstate C, based on prior association with attention-reorientation RSNs) and visual (microstate B, based on prior association with visual imagery RSNs) areas would correlate with individual G*f* profiles, and that changes in G*f* after cognitive training would correlate with modification of the same microstates.

Materials and Methods

Subject Recruitment

Data were collected as part of a study testing the effect of cognitive training on Gf. A total of 74 participants were recruited from the community by online advertisement, and approached by e-mail or by phone. Inclusion criteria included: age 18–65 years, normal healthy volunteer, English native-speaker. Exclusion criteria were: corrected visual acuity <60%; pregnancy; sleep deprivation (less than 6 h a day); history of migraines; history of fainting spells of unknown or undetermined etiology that might constitute seizures; history of seizures, diagnosis of epilepsy, history of abnormal (epileptiform) EEG or family history of treatment resistant epilepsy; contraindication to MRI (e.g. ferromagnetic implant, significant claustrophobia); any implanted medical devices (i.e. cardiac pacemaker, deep brain stimulator, medication infusion pump, cochlear implant, vagal nerve stimulator) unless otherwise approved by the responsible MD; substance abuse or dependence within the past 6 months.

Six subjects did not complete the cognitive training or post-training assessment, therefore the final sample was composed of 68 subjects (38 males, 30 females), with mean age and education of 29 years (range 21 to 49, SD = 12) and 15 years (range 11 to 23, SD = 3) respectively. Four participants were left-handed as suggested by their score at the Edinburgh Handedness Scale. All participants gave written informed consent to the study, which was approved by the Committee for Clinical Investigations at Beth Israel Deaconess Medical Center.

EEG Recording and Data Preprocessing

EEG was recorded using a 20-channel, gel-electrode system from Neuroelectrics (Barcelona, Spain). The system includes 20 leads covering 19 positions of the 10–20 system [Fp1, Fp2, F7, F3, Fz, F4, F8, T3, C3, Cz, C4, T4, T5, P3, Pz, P4, T6, O1, O2] and was recorded at a sampling rate of 500 Hz. Data were collected while the participants sat comfortably with their arms placed on an armrest, eyes open fixating on a crosshair placed on a white wall in front of them. Recording lasted for 5 min and was followed by another 5 min recording while participants kept their eyes closed. Only eyes-open data were used in this study.

Data were imported to MATLAB (vR2012b) using the EEGLAB toolbox (v13.2.1) (Delorme and Makeig 2004). Data were visually inspected and channels showing significant artifacts were manually removed. Power line noise was removed with a notch filter centered at 60 Hz. Data were initially band-pass filtered between 1 and 100 Hz using a zero-phase second-order Butterworth filter. Recordings were divided into 3-second epochs. Ocular and electrode artifacts were removed using a semi-automated procedure utilizing independent component analysis (ICA) as implemented by the ADJUST plugin for EEGLAB (Mognon et al. 2011). Custom scripts were used to remove independent components corresponding to eye movements, electrode discontinuities and muscle artifact. Artifact-obscured channels that had been previously removed were interpolated.

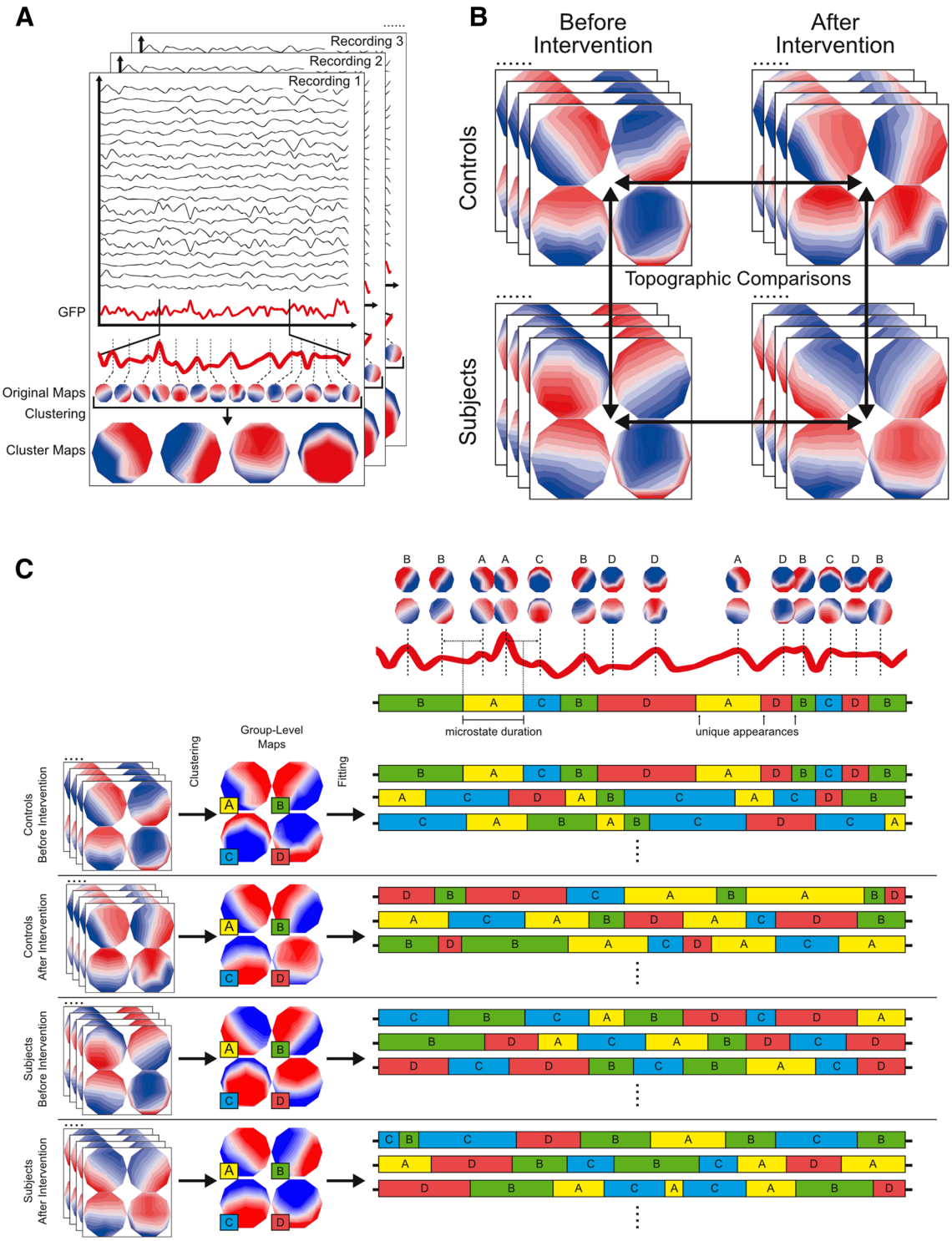

Finally, an additional 30 Hz low-pass filter was applied to the data prior to microstate analysis. Four subjects with EEG recordings containing more than two channels excluded or with persistent significant muscle or electrode artifact after the ICA preprocessing were excluded. This resulted in a final sample of 64 subjects with both pre- and post-intervention EEG recording.

EEG Microstate Analysis

Microstate analysis involves two steps. First, the topographies of the scalp voltage potentials across all electrodes at each time point are collected and submitted to a clustering algorithm to identify clusters of similar topographies over time. Each cluster identified is given an arbitrary label—A,

◂**Fig. 1** Schematic overview of the method of EEG microstate analysis. **a** Each individual EEG recording is initially individually analyzed. First, the GFP at each time point is calculated and plotted to construct a GFP curve for each recording (*red*). Maps at local maxima of the GFP curve represent instances of highest topographic signal-to-noise ratio and are reliable topographic representations of surrounding points in time; therefore, they are selected for further analysis. The maps at all local maxima of the GFP curve are identified as "original maps." All original maps from each recording are submitted to a clustering algorithm individually, and four cluster maps are generated for each individual recording. **b** The four cluster maps generated for each individual recording are used to conduct topographic analysis of variance (TANOVA) to assess for topographic differences in any microstate class across groups or conditions. **c** Cluster maps generated for each individual recording are grouped according to group and condition. Maps in each group are submitted to another round of clustering to generate a set of 4 group-level maps for each group. These group-level maps are fit onto the original data by labeling each original map A, B, C, or D depending on which group-level map it most closely correlates to. Each original recording is ultimately re-expressed as a sequence of these labels, from which values of interest can be calculated. Note that only the map's topography is important, whereas polarity is disregarded in the spontaneous EEG clustering algorithm, i.e. a map and its inverse are considered to be the same. (Colour figure online)

B, C, D, etc. Second, the original sequence of data points is re-expressed as a sequence of cluster labels, assigned based on the cluster membership of each original data point. With the re-expression of the multichannel EEG signal as a time series of cluster labels, properties such as the average length of time for which consecutive maps are assigned to the same label, or the frequency of each label assignment per second can be calculated (Fig. 1).

Microstate analysis was implemented for the current dataset as follows. For each of the 128 individual EEG recordings (64 pre- and post-training), we first identified points of highest topographic signal-to-noise ratio by calculating the global field power (GFP) at each data point. GFP represents the magnitude of the field strength at each moment in time (Lehmann 1971), and is equal to the standard deviation of the average-referenced signal across all electrodes. Topographies that occur at local maxima of the GFP(t) curve represent instants of highest field strength and greatest SNR. Furthermore, EEG topography tends to remain stable around local maxima of the GFP(t) curve, and hence these topographies are representative of topographies at surrounding points in time (Khanna et al. 2014; Lehmann 1971; Yuan et al. 2012). Thus, representation of the original data as a set of topographies at local GFP peaks is a valid method of data reduction. We extracted these topographies at local GFP maxima (hereafter referred to as "original maps") from each of the 128 individual recordings.

Each of the 128 sets of original maps was then individually submitted to a topographic atomize and agglomerative hierarchical clustering (TAAHC) algorithm using the CARTOOL software (Brunet et al. 2011). Details of the TAAHC algorithm can be found elsewhere (Khanna et al. 2014; Lehmann 1971; Yuan et al. 2012). Briefly, the algorithm is comprised of two iterative steps:

1. The quality of each of the n clusters, each comprised of a set of member topographies, is calculated.
2. The lowest quality cluster is eliminated ("atomized"), and its member topographies are reassigned ("agglomerated") to any one of the remaining $n - 1$ clusters.

This process is repeated until the desired number of clusters is obtained.

In our implementation, the quality of each cluster (step 1) was the summated Pearson product-moment correlation coefficient between each constituent map and the "average cluster map." The "average cluster map" was derived by taking the electrode-by-electrode mean of the set of member topographies. Topographic polarity was ignored by inverting member maps of each cluster if correlation with an arbitrarily chosen standard member map was negative. Map reassignment (step 2) was performed by calculating the absolute value of correlation between each map and each "average cluster map," and assigning to the cluster with the highest value. We calculated two clustering quality metrics, the cross-validation (CV) (Pascual-Marqui et al. 1995) and Krzanowski-Lai (K-L) criterion (Tibshirania and Walther 2005), after each iteration of the algorithm to assist in the identification of the optimal number of clusters in the data. Across all 128 individual recordings, CV criteria was minimized at 2.75 ± 0.57 clusters, and the K-L criteria indicated an optimal 4.03 ± 0.39 clusters, suggesting that 3 or 4 clusters would optimally describe the data. This is consistent with a number of prior studies of resting-state EEG that have described optimal clustering with four microstate classes (Khanna et al. 2014; Koenig et al. 2002). Thus, we chose to extract four clusters from each recording.

The data consisted of two subject groups (cognitive training and control) in two conditions (before and after intervention). We collected the four average cluster maps from each EEG recording within each of these four groups and submitted them to another round of TAAHC to derive four group-level representative microstate maps. The four representative microstate maps in each group were labeled A, B, C, and D, and strongly resembled the "archetypal" microstates A, B, C, and D that have been identified in many prior studies (Fig. 1a) (Koenig et al. 2002). In the final step, the microstates A, B, C, and D from each group were fit onto the original maps from all EEG recordings within each respective group. Each original map was labeled A, B, C, or D based on which microstate map had the highest correlation to the original map. Thus, each recording was re-expressed as an alternating sequence of

microstates A, B, C, and D. From these microstate time series, for each microstate, we calculated the average microstate lifespan, frequency of appearance, fraction total covered time, and the average number of consecutive original maps (occurring at GFP peaks) assigned to each microstate class when it appears ("GFP peaks/appearance"). The lifespan of each microstate was calculated as the time during which all successive original maps were labeled as the same microstate, starting and ending halfway between the last original map of the preceding microstate and the first original map of the following microstate, respectively. The frequency of each microstate was the number of new appearances of each microstate per second. The fraction total covered time of each microstate was the percentage of total time that is spent in each microstate class. Note that these values are not completely independent. We compared these values between the two groups and conditions, and determined the correlation between these values and G*f*.

Fluid Intelligence Measurement

In an effort to obtain a task-independent measure of G*f*, we measured performance on three different G*f* tasks—Raven's Advanced Progressive Matrices (RAPM) (Raven et al. 2003), Sandia matrices (Matzen et al. 2010) and Bomat (Hossiep et al. 1999)—and applied a dimensionality reduction procedure based on principle component analysis (PCA).

RAPM is the most commonly employed abstract reasoning test and provides a domain-independent measure of fluid reasoning by sampling from both verbal-analytic and visual-spatial domains, which together underlie performance on many cognitive tasks. The performance on RAPM is considered to be the best estimate of the general factor of intelligence (*g*) (Gray and Thompson 2004b). One of the most limiting factors of current approaches for longitudinal G*f* assessment is the limited number of available RAPM stimuli, with consequent difficulties in the case of cognitive training. In this study, two balanced lists of matrices have been created for Pre-Post testing, by using individual accuracy values obtained in a longitudinal study on a separate sample (Thompson et al. 2013).

Sandia Matrices are a recently created set of stimuli for G*f* testing, which were intended to solve the aforementioned numerosity issue, by providing approximately 3000 matrices obtained through the combination of different stimulus features like shape, color and orientation, as well as offering the possibility to discriminate the stimuli on the basis of the type of reasoning process involved. Given that performance on specific tasks is subserved by partially distinct structures (Prado et al. 2010), specific Sandia matrices allow one to address diverse cognitive processes. Trials more related to prefrontal activation (i.e. Sandia Logical matrices, Sandia-LOG) involve conditional arguments (e.g. Modus Tollens: if P then Q; not-Q), while others referring to tasks about the formulation of relational syllogisms (i.e. Sandia Relational matrices, Sandia-REL) (e.g. P is to the left of Q; Q is to the left of R) rely on posterior areas, such as the temporo-parietal-occipital junction (Prado et al. 2010). Experimental matrices belong to 4 different classes based on the type and number of analogical operations required for a correct solution (1-, 2-, 3-Relations and Logic matrices). For the present study, subjects were tested using 3-Relations and Logic matrices only, given the ceiling effect often observed with the remaining 1- and 2-relations trials. The structure of Sandia Matrices closely resembles the RAPM, with the upper part composed of a 3×3 stimuli grid, and the lower one with eight possible response choices numbered from 1 to 8. Each grid presents a blank cell (position 3–3, i.e. the lowest one on the right), which must be filled in using one of the 8 alternatives. Two separate lists of 45 stimuli balancing LOG and REL stimuli were prepared and used for baseline and follow-up evaluation after the training.

The Bomat task was originally developed in order to address fluid intelligence capacity in the high performance range. Similar to the RAPM and Sandia, it is a language-free method that detects logical-deductive reasoning by using visual stimuli arranged in a matrix-like solution. In each test item, the subject is asked to identify the missing item that completes a pattern of a 5×3-field matrix, choosing from six options. For the current protocol the "advanced-short" version of Bomat has been used and two lists of stimuli were created by dividing the stimuli as specified in the test manual.

Identification of Task-Independent Components of Fluid Intelligence

Given the multidimensional nature of intelligence, the definition and measurement of an individual's intelligence level itself requires a thorough assessment in order to get a reliable estimate (Cole et al. 2004; Colom et al. 2013; Engle et al. 1999). Therefore, the aforementioned three independent Gf measures (RAPM, Sandia [LOG and REL], Bomat) were analyzed using a PCA procedure based on Varimax rotation (Kaiser 1958) applied on the correlation matrix. Since LOG and REL trials may index distinct cognitive processes (Matzen et al. 2010) and rely on the activity of different brain regions (i.e. higher load on prefrontal lobes for LOG, higher parietal load for REL) (Santarnecchi et al. 2013, 2016a), the scores at Sandia-REL and LOG were included separately in the PCA analysis. Scores obtained for the RAPM, Sandia-LOG, Sandia-REL and Bomat at baseline were: [RAPM] range 35–100% (mean 77%, standard deviation 14%); [Sandia-LOG] range 19–94%

(mean 69%, standard deviation 19%); [Sandia-REL] range 18–82% (mean 57%, standard deviation 16%); [Bomat] range 7–100% (mean 54%, standard deviation 23%). A data-driven selection of the number of components was applied, resulting in a two-component solution as depicted in Fig. 2a (Component 1 Eigenvalue = 3.355, Component 2 Eigenvalue = 1.24; total variance explained = 81%; Component 1 = 58%, Component 2 = 23%). The first component (Gf-1, red) includes scores from the RAPM and Sandia-LOG tasks, the second one (Gf-2, blue) includes Bomat and Sandia-REL scores. All subsequent analyses were run on individual scores calculated as weighted values applying Bartlett transformation (Fig. 2). The Bartlett method uses the least squared procedure to minimize the sums of squares of the factors over the range of variables. It is preferable because of its univocality (each variable is highly correlated with one factor only), thus leading to simpler structures, which eases interpretation in correlational studies (Bartlett 1937). The scores on each G*f* task did not show any gender related differences (Fig. 2d).

Cognitive Training

An ad-hoc, adaptive, computer-based executive-function training program was developed for the study. Even though the current literature about cognitive training is mostly

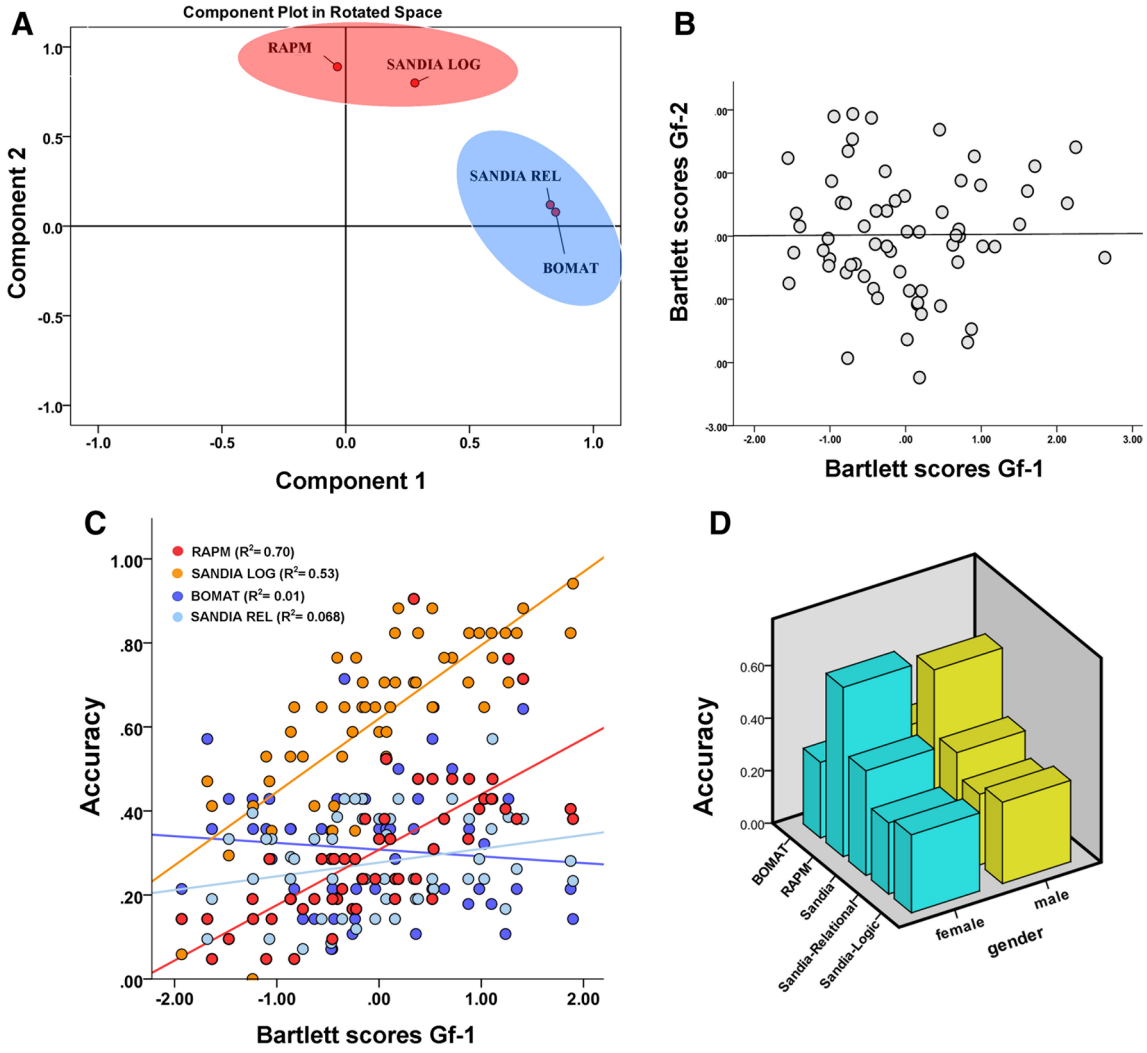

Fig. 2 Fluid intelligence components at the latent variable level. Panel **a** shows the loading of each fluid intelligence task in the rotated space obtained using principal component analysis (PCA), with the two components respectively highlighted in red and blue. **b** Resulting individual Bartlett scores for the PCA components show a separation of the two G*f* components by means of a Pearson "r" coefficient close to 0. **c** Correlations between G*f*-1 and accuracy levels for each Gf task highlight the loading of RAPM and Sandia-LOG scores on G*f*-1 in the overall sample at baseline (*red* and *orange dots* respectively). **d** Mean scores for the fluid intelligence tasks show no gender related differences. Note: straight lines represent a linear fit for the different data, with the percentage of explained variance reported using R squared values. (Colour figure online)

focused on interventions uniquely based on working memory (WM) training (Au et al. 2014), both behavioral and neuroimaging studies show overlap between G*f* and WM, response-inhibition and task-switching functions (Benedek et al. 2014; Dang et al. 2014; Hambrick and Altmann 2015; Zook et al. 2004), suggesting a rationale for the implementation of training interventions targeting all three of these dimensions. A video-game based on multiple executive function tasks addressing WM, response-inhibition and task-switching was developed by SIM-COACH GAMES (http://www.simcoachgames.com/), with a progression algorithm aimed at unlocking new levels only when a specific proficiency level was achieved. The game initially presented participants with unimodal repeated trials (~2 min each) of tasks involving either response inhibition (via a stop-signal task), task-switching (e.g. switch cost test), or working memory updating (*n*-back task). The game kept presenting trials belonging to a specific category until the participant reached a certain proficiency level (accuracy and/or reaction time threshold). Subsequent trials were composed of tasks integrating two executive functions at the same time (e.g. updating and inhibition), resulting in three possible trial types (update and inhibition, inhibition and switching, switching and updating). The final levels in the game included trials based on logical and relational operations (e.g. Boolean operators like AND, OR, XOR), for a more direct training of abstract-reasoning skills. Integration of logical operations and executive functions trials were also presented at the higher difficulty levels in the game. Performance was monitored for each trial/session, adjusting the difficulty of following trials as well as unlocking new levels in real time. The training was composed of ten 30-min long daily sessions over the course of two weeks (excluding weekend days). Participants underwent a brief explanation of the training before the first session and then received hints and suggestions during the training when needed.

It should also be noted that some participants also underwent non-invasive transcranial current stimulation (tCS) (Filmer et al. 2014; Santarnecchi et al. 2015a) during the training program. The stimulation took place while participants were playing the cognitive-training game, and was aimed at amplifying its effect. Different participants underwent different tCS interventions (transcranial random noise stimulation—tRNS, n = 13; transcranial direct current stimulation—tDCS, n = 10; multifocal tDCS, n = 8; trancranial alternating current stimulation—tACS, n = 7).

This study is specifically focused on (i) identifying baseline neurophysiologic correlates of Gf and (ii) verifying that changes in Gf as a result of an intervention (in this case, a cognitive training program) are associated with changes in the same neurophysiological metrics identified as baseline correlates of Gf. Therefore, further details of the cognitive training program and detailed analysis of cognitive training results are beyond the scope of this manuscript, and will be reported separately (McKanna et al. in preparation). However, the specific training and stimulation regimen experienced by each participant is included in the statistical design as a covariate.

To ensure that changes in microstates were not simply due to a limitation in test–retest reliability, a control group (n = 26; 14 males, 12 females; mean age 27 years [range 20 to 45, SD = 9]; mean education 14 years [range 10 to 21, SD = 3]) received the same pre-post EEG recording and cognitive evaluation while not undergoing any cognitive training ("control group"—CG hereafter). The two groups (CT and CG) did not differ in terms of age and gender distribution. Pre-post evaluations were separated by 3 weeks on average.

Baseline Correlates of Fluid Intelligence

Analyses were carried out using IBM SPSS Statistics (Version 21, release 21.0.0) and MATLAB (Release 2012b, Mathworks). The correlations between Gf scores and (i) the features extracted for each microstate (average life, frequency, coverage, and GFP peaks/appearance) and (ii) the general properties of the state space (global GFP peaks/second, global frequency, global average life) were calculated using Pearson product-moment coefficients independently for each Gf Factor. Results are displayed for the analysis on the entire sample (n = 64) as measured before the cognitive training intervention, with $\alpha = 0.05$ corrected for multiple comparisons using Bonferroni correction. Even though evidence about the non-random nature of the transitions between microstates (e.g. the probability of switching from state A to state B, so called Syntax analysis) has been published (Lehmann et al. 2005), our analysis failed at demonstrating transitions being non-randomly distributed. Therefore, information about syntax has not been included in any statistical model.

Changes in Fluid Intelligence and Microstates Properties with Cognitive Training

Two separate repeated measures Analysis of Covariance (rm-ANCOVA) including factors "TIME" (two levels, Pre & Post) and "INTERVENTION" (two levels, CT and CG) were calculated, respectively including behavioral scores (Gf-1 and Gf-2 Bartlett's scores for all participants before and after intervention) and microstates properties (i.e. frequency, coverage, average life, GFP peaks) as well as general properties of the state space (global GFP peaks/second, Global frequency, Global average life). Values for gender, age, education and tCS montage were included as covariates in the model. In the event of a significant effect

of TIME or INTERVENTION, further simple main effects were analyzed using a similarly structured ANCOVA to decompose the effect. Post-hoc comparisons were calculated for each pair applying the Bonferroni correction for multiple comparisons. For all tests the level of significance was set at $p \leq 0.05$.

Microstate Topographic Changes with Cognitive Training

The impact of cognitive training on microstates structure was evaluated with a topographic analysis of variance (TANOVA) test to compare each microstate class (A, B, C, and D) among the two subject groups in the two conditions (CT vs. CG). TANOVA utilizes randomization statistics to test the magnitude of the difference between two groups of maps against the null hypothesis that the assignment of maps to groups is random (Koenig and Melie-Garcia 2009). The two groups of maps to be compared are each electrode-by-electrode averaged to produce two group-averaged maps. The test statistic representing the magnitude of the difference between these two group-averaged maps is the global map dissimilarity between them:

$$GMD(u,v) = \sqrt{\frac{\sum_{i=1}^{n}\left(u_i - v_i\right)^2}{n}}$$

where u_i' and v_i' are the potentials at electrode i in the maps being compared.

After the actual test statistic is calculated, the maps are randomly shuffled between the two groups, and the test statistic is recalculated. This process is repeated 5000 times to generate a distribution of test statistics under the null hypothesis that the maps are randomly distributed between the two groups. The fraction of test statistics greater than the actual test statistic is the p value.

Statistical association between map topography and a linear predictor can also be ascertained using the related topographic analysis of covariance (TANCOVA) test. In TANCOVA, so-called "covariance maps" are calculated, given a set of u maps with i electrodes, and linear predictors b for each observation j:

$$\beta_j = \sum_{i=1}^{m} v_{ij} \cdot b_i$$

In this case, the test statistic is:

$$s = \sqrt{\frac{\sum_{j=1}^{n}\left(\beta_j - \bar{\beta}\right)^2}{n}},$$

where

$$\bar{\beta} = \sum_{j=1}^{n} \beta_j$$

Similarly, the assignments between maps u and linear predictors b_j are randomly shuffled, and s is recalculated 5000 times; the proportion of test statistics greater than the actual test statistic is the p value of association between topographic change and the linear predictor b.

Source Localization of Topographic Changes with Cognitive Training

To localize changes in intracranial current source densities that could produce microstate topographic changes, exact low resolution brain electromagnetic tomography (eLORETA; Pascual-Marqui 2007) implemented in LORETA-Key software (http://www.uzh.ch/keyinst/loreta.htm) was used to identify changes in cortical three-dimensional distributions of neuronal activity associated with changes in microstate topographies. The eLORETA algorithm is an inverse solution with exact localization in the presence of measurement and structured biological noise (Pascual-Marqui 2007). Computations were performed using a head model based on the MNI152 template (Mazziotta et al. 2001), with three-dimensional solution space restricted to cortical gray matter, as determined by using the probabilistic Talairach atlas (Lancaster et al. 2000). The solution space was comprised of 6239 voxels at 5 mm spatial resolution.

For microstates with significant topographic changes identified with TANOVA, eLORETA current source densities (assuming a signal-to-noise ratio of 5) were calculated separately for each recording. The logs of ratio of averages of current source densities before and after cognitive training in a paired fashion by subject were compared for each 6239 voxels. Significant differences in current density at each voxel were assessed by statistical nonparametric mapping randomization, which determines the threshold log ratio of averages between the two compared groups that reaches critical significance threshold with $p < 0.05$ after correction for multiple comparisons across all voxels (Nichols and Holmes 2002).

Interaction Between Microstate and Behavioral Changes after Cognitive Training

Differences in the Bartlett scores obtained before and after the cognitive training were calculated for G*f*-1 and G*f*-2 in the entire sample, and correlated with changes in microstate properties (frequency, coverage, average life, GFP peaks) and general properties of the state space (global GFP peaks/second, Global frequency,

Global average life). Differences in both microstate and behavioral scores were calculated subtracting baseline scores from post-intervention ones, resulting in an index displaying positive and negative values for, respectively, increase and decrease in the feature at hand. Post-intervention fluid intelligence data were extracted using the PCA-based weights obtained on pre-intervention data of the same sample. The level of significance was set at $p \leq 0.05$ (Bonferroni correction for multiple comparisons).

Results

Baseline Correlates of Fluid Intelligence

As described in the "Materials and Methods" section, PCA analysis revealed two separate G*f* sub-components in the behavioral data, representing two Gf factors respectively indexing executive functions (G*f*-1) and activity in the visual system (G*f*-2). This dual structure allowed for potential interactions between specific brain states and cognitive abilities tapping on different domains related to G*f* to be investigated. As shown in Fig. 3, the correlation between Gf factors and microstates properties revealed distinct patterns for Gf-1 and G*f*-2. There was a significant negative correlation for G*f*-1 with the frequency of Microstate C ($r = -0.503$, $p < 0.002$) and with a global property of the state-space, i.e. GFP peaks/sec ($r = -0.451$, $p < 0.008$). For G*f*-2 we found a negative correlation with the frequency of Microstate B ($r = -0.346$, $p < 0.012$). No other significant correlations between baseline Gf factors and EEG microstates were identified. See Supplementary Table 1 for the detailed results of the microstates analysis, and Supplementary Table 2 for the full set of correlation coefficients.

Behavioral Differences in Fluid Intelligence after Training

The rm-ANCOVA revealed significant effects of TIME [$F_{(1,132)} = 4.376$, $p < 0.05$] and INTERVENTION [$F_{(1,132)} = 4.931$, $p < 0.01$], with a significant interaction between the two factors [$F_{(1,132)} = 4.74$, $p = 0.023$]. The simple main effect of TIME was significant for G*f*-1 [$F_{(1,132)} = 9.79$, $p < 0.01$; Pre-Post increase +16%] and G*f*-2 [$F_{(1,132)} = 7.43$ $p = 0.009$; Pre-Post increase +28%] (Fig. 4a). The simple main effect of INTERVENTION was significant only for G*f*-2 [$F_{(1,132)} = 4.73$, $p = 0.019$]. The significant interaction term was driven by a Pre-Post difference in G*f*-2 scores observed for the CT group but not for participants in the CG [$t_{(61)} = 3.92$, $p = 0.012$].

Cognitive Training Alters the Topography of a Specific Microstate Class

Individual microstate topographies are thought to emerge from the activity of underlying brain networks. To identify whether cognitive training affects microstate topographies, we extracted a set of four microstates from each subject before and after intervention. These topographies were each labeled A, B, C, and D depending on the degree of correlation between each map and the "archetypal" maps A, B, C, and D that have been identified in many previous studies (Khanna et al. 2014; Koenig et al. 2002). The set of maps A, B, C, and D were compared across conditions using TANOVA as described in "Materials and methods" section. There were no significant differences between the topographies of A, B, C, or D between controls and subjects who underwent training at baseline ($p > 0.05$ for

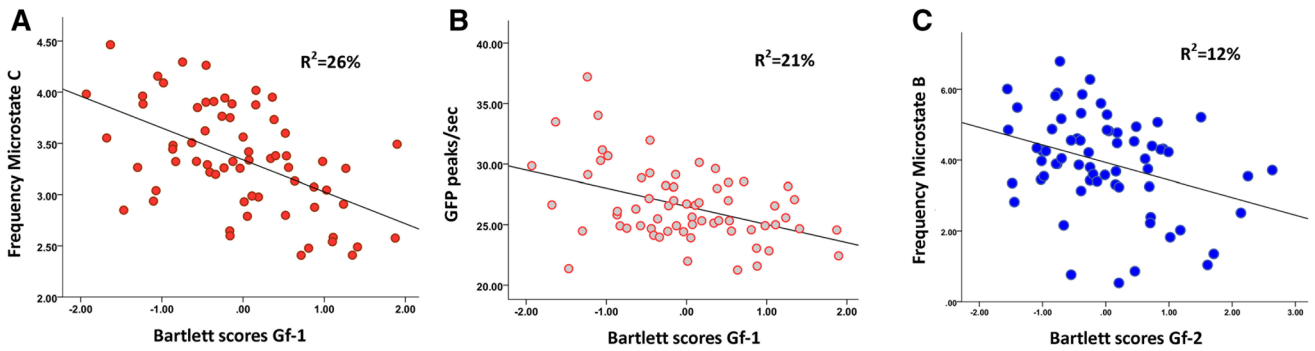

Fig. 3 Baseline correlation of fluid intelligence with microstate features. **a** Significant negative correlation between Bartlett scores derived for the first component (G*f*-1) and the frequency of appearance of microstates C. **b** G*f*-1 also showed a significant negative correlation with the number of GFP peaks per second. **c** Significant correlations between Bartlett scores for G*f*-2 and the frequency of microstate B. Note: *straight lines* represent a linear fit for the different data, with the percentage of explained variance reported using R squared values

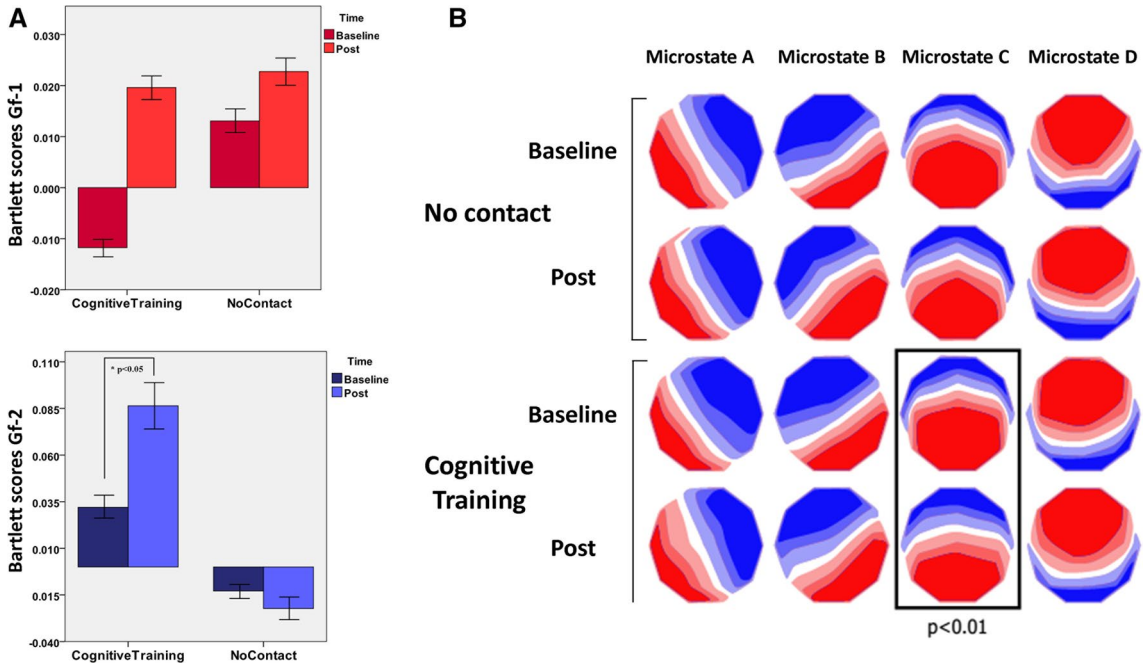

Fig. 4 Behavioral and topographic differences before and after intervention in controls and trained subjects. Panel **a** reports the comparisons between the Bartlett scores for the two G*f* factors calculated before and after the intervention in the two groups. A significant effect of cognitive training is observed for G*f*-2 in the cognitive training group (*). **b** Original maps at local maxima of the GFP curve for each EEG recording were submitted to a topographic clustering algorithm to derive four representative microstate maps for each recording. Maps in each set of four were labeled A, B, C, and D depending on their topographic correlation with the "archetypal" microstates A, B, C, and D that have been described in numerous prior studies. These sets of maps from individual EEG recordings were compared using the topographic analysis of variance (TANOVA) randomization statistical test. The microstates A, B, C, and D shown for each group represent electrode-by-electrode averages of all microstates of the given class within each group. TANOVA revealed a significant difference in the topography of microstate C after cognitive training ($p < 0.01$). No other significant topographic differences were identified. (Colour figure online)

each comparison between maps A, B, C, and D). Controls did not show any significant difference in topographies 3 weeks after baseline evaluation. However, among subjects who underwent cognitive training, there was a significant difference in microstate C following the intervention ($p = 0.0064$). Topographically, this corresponded to a more posterior isoelectric point in the map of microstate C after cognitive training (Fig. 4b). No other significant differences among groups were found.

To determine whether the topography of microstate C was linearly correlated with G*f*-1 or G*f*-2, we calculated TANCOVA using G*f*-1 and G*f*-2 separately as linear predictors for the topography of microstate C. Neither factor demonstrated a statistically significant association with microstate C using TANCOVA.

We used eLORETA to identify changes in intracranial current source densities that could explain the change in microstate C topography observed after cognitive training. Statistical comparison between source localizations of microstate C of subjects before and after cognitive training revealed a pattern of increased current density in left parietal and occipital regions, whereas a decrease was observed in the right inferior frontal gyrus and insular region (Fig. 5; threshold: log-F = 0.874, $p < 0.01$).

Changes in Microstates Properties After Training

This analysis revealed significant effects of TIME [$F_{(1,132)} = 8.749$, $p < 0.01$], whereas a significant interaction between TIME and INTERVENTION was not present [$F_{(1,132)} = 0.43$, $p = 0.253$]. The simple main effect of TIME was significant for the average life of both microstate C [$F_{(1,132)} = 10.92$, $p < 0.006$; increase + 8.2%] and microstate D [$F_{(1,1325)} = 7.91$, $p < 0.002$; decrease −9.8%] (see Fig. 6a, b), with similar but not statistically significant results also for frequency and coverage values of the same microstate classes.

Correlation Between Changes in Microstates and Behavioral Scores

Differences in Bartlett scores obtained before and after the cognitive training were calculated (for G*f*-1 and G*f*-2). We then correlated these scores with changes in microstate

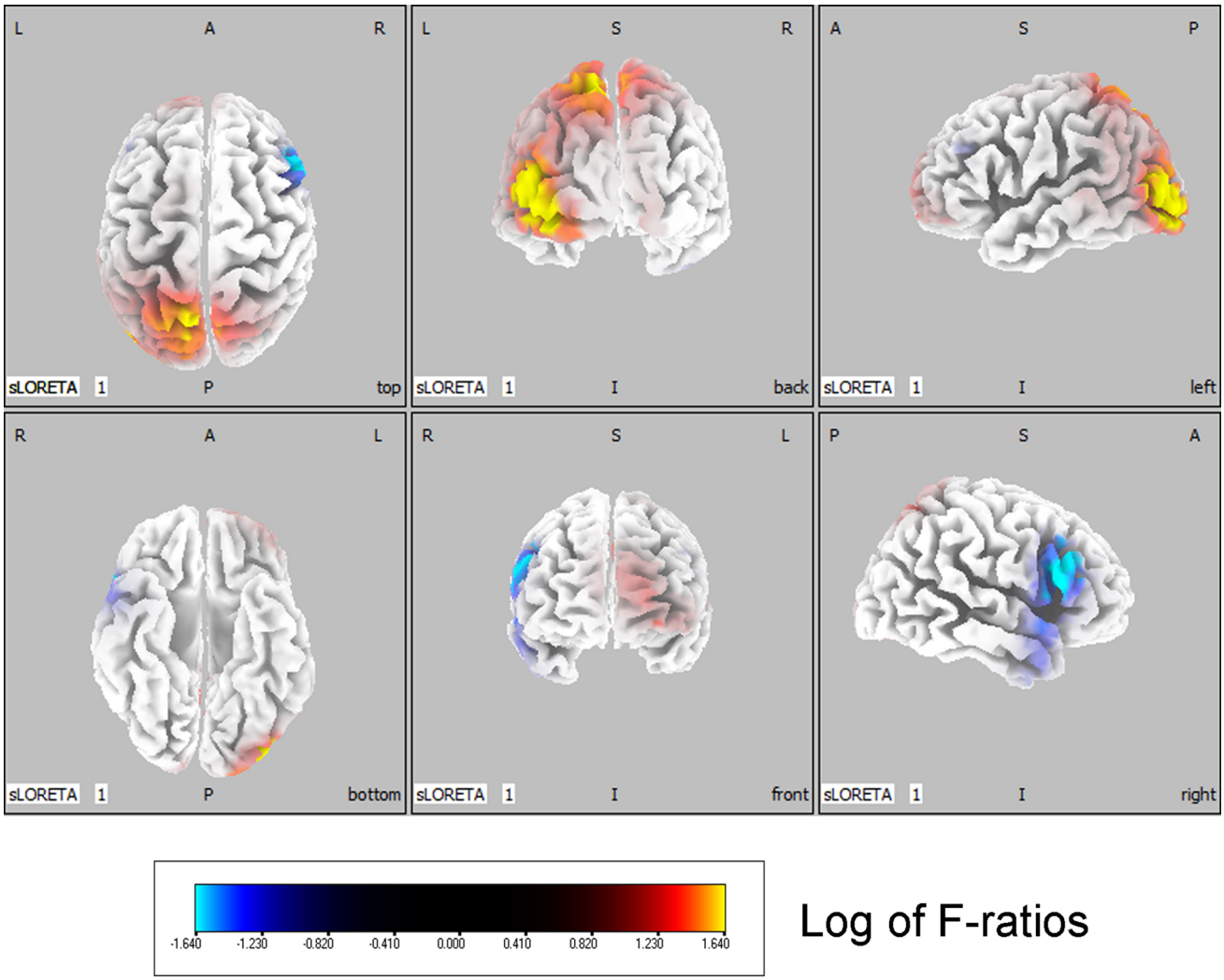

Fig. 5 eLORETA statistical map of change in current source power after cognitive training. Colored areas represent the spatial extent of voxels with a significant difference in current source density after cognitive training for Microstate C (*red*-coded for regions that show significant increase, *blue*-coded for regions that show a significant decrease; $p < 0.01$, corrected for multiple comparisons), projected onto a fiducial cortical surface. The color scale represents log F-ratio values (threshold: log-F = 0.874, $p < 0.01$). (Colour figure online)

properties (frequency, coverage, GFP peaks) for states A, B, C and D in both the CT and CG groups. A significant negative correlation was identified for the coverage of state B and changes in G*f*-2 in participants undergoing the cognitive training ($r = -0.379$, $p < 0.012$) (Fig. 6c).

Discussion

Human intelligence has been related to several intrinsic properties of the human brain, which can be measured with neuroimaging and electrophysiological techniques. An emerging consensus emphasizes the role of brain regions functionally organized into distributed, large-scale networks that facilitate progressively higher orders of cognitive processing which collectively constitute intellectual ability (Jung and Haier 2007; Vakhtin et al. 2014). In the present study, we employed EEG microstate analysis, which provides spatiotemporal insights into the activity of large-scale cortical networks, to study fluid intelligence, G*f*. We hypothesized that G*f* would be most closely related to microstate features associated with visual networks (reflecting low-level visual/perceptual processing loading on occipital and parietal regions), as well as microstate features associated with prefrontal activation (reflecting higher-level cognitive processing, such as cognitive control). Furthermore, we hypothesized that improvement in G*f* after cognitive training would be reflected by changes in microstate features specifically limited to these networks. Our data confirm our hypotheses by showing that

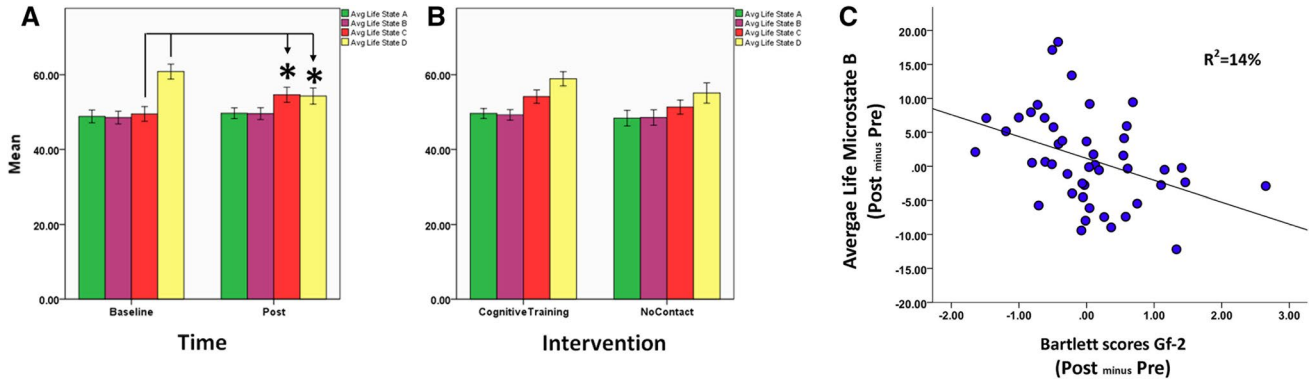

Fig. 6 Training effects on microstates properties. Panel **a** and **b** report results of the repeated-measures-ANCOVA run on the average lifespan values of each microstate class. The only significant results were related to the effect of TIME on the average lifespan of microstate C and D (*), with no significant differences between participants in the cognitive training and no-contact group. No significant results were identified for the interaction between TIME and INTERVENTION, as well as for the remaining microstates properties (e.g. frequency, coverage, GFP peaks). **c** *Scatterplot* displays the negative correlation between changes in microstates properties and fluid intelligence scores after training, with the average life of state B being inversely correlated with changes in G*f*-2 in the group receiving cognitive training. No other correlation coefficients reached the significance level ($p < 0.05$ Bonferroni corrected for multiple comparisons). (Colour figure online)

G*f* is inversely correlated with specific properties of microstates B and C, which have previously been shown to load on occipital and prefrontal regions, respectively (Britz et al. 2010b). A shift in topography of state C was observed after a cognitive training intervention aimed at increasing fluid intelligence, which was associated with increased current source density in left parietal and occipital lobes, as well as decreased density in the right inferior frontal gyrus and insula. Separation of G*f* into two independent components revealed that components Gf-1 and Gf-2 were specifically correlated with microstate C and B respectively, suggesting that these microstates represent distinct cognitive processes tapping on subcomponents of abstract reasoning. Finally, improvement in Gf-2 after cognitive training was significantly correlated with reduction in the stability (i.e. average lifespan) of microstate B.

The present results suggest a pivotal role for brain regions related to visual processing and executive control networks in G*f*, and compellingly demonstrate how external interventions (in this case, aimed at cognitive enhancement) offer a powerful approach to identify robust neurophysiological correlates of human cognition.

Fluid Intelligence and Activity in Visual and Cognitive Control Regions

The multidimensional nature of intelligence has been shown to poorly fit with data obtained from single task evaluations, making G*f* assessment difficult when using only a single measurement with a standardized tool (Beaujean et al. 2010; Cole et al. 2004). Our data show how assessing G*f* using three different validated tasks in a fairly large sample of healthy individuals might result in the identification of more than one factor accounting for individual variability in G*f*. Specifically, Bomat and Sandia-REL scores load on a different factor than scores from the RAPM and Sandia-LOG. This distinction may be due to the physical properties of the stimuli themselves, which is reflected in a correlation with distinct EEG microstates.

The first G*f* component, whose score is driven by RAPM and Sandia-LOG scores, is (inversely) associated with the frequency of microstate C. The specific network activations that result in a given microstate pattern are not clearly defined. One previous study examining the resting-state network correlates of microstates A, B, C, and D have concluded that microstate C is most closely associated with the salience network, most specifically with the activity of the anterior cingulate cortex (ACC), bilateral inferior frontal gyri, right anterior insula, and left claustrum (Britz et al. 2010b). This pool of regions includes cortical and subcortical structures representing crucial nodes for executive functioning (e.g. ACC) and processing of logical/conditional rules (e.g. bilateral inferior frontal gyrus, middle frontal gyrus). Such functions have been repeatedly associated with performance at RAPM and other abstract reasoning tasks (Crone et al. 2009; Gray et al. 2003; Perfetti et al. 2009), with functional studies suggesting gray matter volume and regional homogeneity values of regions belonging to the salience network to be significantly correlated with G*f* as measured by RAPM (Yuan et al. 2012).

The second G*f* component—indexing Bomat scores and relational trials of Sandia—is related to microstate B. Work by Britz and colleagues has associated microstate B with BOLD activity in bilateral extrastriate visual areas

(BA18 and BA19) (Britz et al. 2010b), regions known to be involved in spatial attention (Bondarenko et al. 2012; Martinez et al. 1999; Peters et al. 2012). This suggests a tighter link between performance on Bomat/Sandia-REL and spontaneous activity of the parieto-occipital cortex, possibly reflecting the higher involvement of abilities related to visual search, feature selection and visuospatial attention, rather than more prefrontal abstract-reasoning abilities (e.g. rule inference). It should be noted that Bomat matrices are composed of a more dense array of stimuli than Sandia (i.e. 5×3 *vs*3×3 grid) which might elicit a larger involvement of visual areas during the early stages of problem solving (i.e. scanning phase) (Carpenter et al. 1990), and consequently a higher visual working memory load to retain such additional items during the subsequent rule inference and response generation processing stages. As suggested previously (Moody 2009), this might indicate that Bomat—and Sandia-REL as well, although the stimuli are less spatially dense—engage specific subcomponents of G*f* related to visuospatial working memory and filtering ability rather than pure abstract/logic reasoning processes (Burgess et al. 2011).

We note that microstate analysis is most often derived from EEG data collected with the eyes closed, whereas our analysis was conducted on data collected with the eyes open. However, as the topography of the microstates seen in our data is generally consistent with the prior literature (including the work of Britz et al. 2010b), this difference should not impact the interpretation of the relevant activated networks. Therefore, our findings regarding microstate C may reflect an association between the cognitive control network and higher-level processes composing fluid intelligence, while the involvement of microstate B may implicate extrastriate visual cortical recruitment in visuospatial aspects of G*f* processing.

Higher Fluid Intelligence, Reduced Microstate Activations

The observed negative correlation between specific microstate properties and G*f* offers novel insights on the neurobiology of G*f*. The frequency of appearance of a microstate class represents the propensity for its underlying neural generators to become activated (Khanna et al. 2015). Thus, our results suggest that increasing G*f*-1 and G*f*-2 scores correlate with relatively reduced resting-state engagement of the networks underlying microstate C and B, respectively. There are two possible explanations for these inverse associations. First, this may represent a form of so-called "neural efficiency," whereby lower activity of the network in the resting state represents heightened efficiency and enables better performance during a cognitive task (Micheloyannis et al. 2006; Neubauer and Fink 2009). In our subjects, lower spontaneous recruitment of microstate B or C at rest may represent more "reserve" to be exploited during relevant cognitive engagement. Alternatively, these individuals may have lower activation of networks underlying microstate B or C in general, due to greater network efficiency regardless of cognitive demand (Neubauer et al. 2004; Santarnecchi et al. 2014).

A second potential explanation for the negative association between Gf scores and the frequency of microstates B and C was recently proposed by Milz et al. (2015), who remarked that oscillations within the alpha band, which dominates the frequency bandwidth from which microstates are calculated, typically represents inhibitory rather than excitatory control on modality-specific processing. The authors postulated that decreasing microstate activity might actually reflect disinhibition of the underlying brain regions and corresponding cognitive processes (Milz et al. 2015). Alternatively, they suggest that decreasing activity of a given microstate class could represent release of tonic inhibition by brain regions corresponding to that class on other brain regions or processes. Therefore, our finding of decreasing frequency of microstate C correlating with increasing G*f*-1 may reflect reduced inhibition of frontal control networks (e.g. ACC, inferior/middle frontal gyri), or may reflect reduced inhibition by frontal control networks on others. Similarly, decreasing activation of microstate B, which shows a right-posterior source (i.e. parieto-occipital; Pascual-Marqui et al. 2014), may be associated with disinhibition of areas related to visuospatial processing—such as the right posterior parietal cortex (Malhotra et al. 2009)—correlating with increasing G*f*-2 scores.

Moreover, Milz and colleagues also related individual microstate classes with particular modalities of thinking, specifically "object visualization," "spatial visualization," and "verbalization", compared to rest. Interestingly, the authors report that both object and spatial visualization were associated with decreased duration of microstate C, while the frequency, duration, and coverage of microstate B was decreased in spatial visualization compared to verbalization. If decreasing microstate activity indeed represents disinhibition of corresponding underlying brain regions, these results are consistent with our findings relying on a G*f* assessment based on culture-fair tasks, which load on object and spatial visualization more than verbalization (Kush et al. 2012; Verney et al. 2005).

Our findings of negative association between the frequency of microstates C and B with G*f* is also interesting in the context of other studies of microstate changes in neuropsychiatric disease. For example, several studies have found that patients with schizophrenia (or with genetic susceptibility to schizophrenia, e.g. 22q11.2 deletion syndrome) have higher frequency of microstate C compared to healthy subjects (Tomescu et al. 2014; Nishida et al.

2013; Lehmann et al. 2005), which has been suggested to be related to aberrations in resting-state networks mediating salience processing that is known to be dysfunctional in schizophrenia (Nishida et al. 2013). These studies raise the intriguing possibility that the converse is true in our dataset—that decreased frequency of microstate C is somehow associated with increased activity of the salience network. Aberrations in microstate C and B have been identified in other disorders as well (Khanna et al. 2015), but only in single studies, and relation to our findings remains speculative.

Clearly, such precise association between specific microstates and behavior requires much additional validation, and should be interpreted carefully. Regardless of a putative role assigned to a given state, each behavioral or mental modality always implies the co-existence of all microstates classes identified so far (Milz et al. 2015), making their interplay and the ratio between their contributions to ongoing brain processing central to understanding the electrophysiological mechanisms supporting G*f*. Further studies evaluating microstate syntax during abstract-reasoning processes (e.g. during rule inference and response generation phases) (Carpenter et al. 1990) could confirm and expand on current findings.

Enhancing Cognition by Modulating Inhibition?

Participants exposed to cognitive training had a significant increase in G*f*-2 scores, while no such improvement was seen in control subjects who did not undergo cognitive training. Notably, the cognitive training group had a change in the topographic map corresponding to microstate C, characterized by a posterior shift in the isoelectric point. In addition, the degree of G*f*-2 improvement after training was negatively correlated with the change in the stability (i.e. average lifespan) of microstate B (Fig. 6c). The negative correlation between changes in the average lifespan of microstate B and G*f*-2 scores after training is consistent with the context highlighted by Milz and colleagues (Milz et al. 2015). It also supports the association between microstate B and cognitive modalities related to G*f*-2 that were identified at baseline in our dataset. Specifically, as discussed above, better baseline G*f*-2 scores could be related to decreased resting-state inhibitory activity in posterior visual processing regions (Buschman et al. 2011; Soulieres et al. 2009). Therefore, the negative correlation between changes in microstate B life span and the improvement in G*f*-2 scores suggests that a training-associated decrease in inhibitory processes in visual regions–captured by microstate B activity—is associated with (and may underlie) improvement on the Bomat and Sandia-REL G*f* tasks (in our data, G*f*-2). However, whether the changes in microstate B activity are causally related to the improvement in task performance cannot be assessed.

The interpretation of changes in microstate C topography is more complex. We suggest that our finding of a more posterior centroid for microstate C after cognitive training might be consistent with integration of more posterior regions with the frontal executive/control networks, typically thought to be involved in microstate C activity (Britz et al. 2010b; Oelhafen et al. 2013). Interestingly, prior studies assessing the impact of various forms of cognitive training (e.g. based on inhibition or task switching abilities) have shown a shift in the pattern of fMRI activations after training, describing an increased prefrontal activation with corresponding reduction in contribution from parietal regions (Houde et al. 2000). This dynamic rearrangement of cognitive resources, pointing towards a switch from the "perceptual to the logical brain" (Houde et al. 2000), might fit with the posterior displacement observed in our data, as a reflection of a potential increase in frontally mediated inhibitory control towards posterior regions (Aron et al. 2014; Prado and Noveck 2007). Such prefrontal inhibition has been demonstrated as fundamental for the suppression of irrelevant distractors during working memory tasks (Gaspar and McDonald 2014; Jacob and Nieder 2014; Melara et al. 2012; Pereira and Wang 2015). Our findings support the idea that the same principle might apply to G*f* related processing. Indeed, other studies have indirectly supported such a hypothesis by showing how regions involved in inhibitory control (e.g. dorsolateral, inferior and medial prefrontal cortices) are more engaged when participants successfully overcome perceptual mismatches—a process engaging the parietal lobes—in order to provide a logical response (Prado et al. 2008). This view also fits with the results of our source analysis on microstate C changes with cognitive training, which show an increase in parietal and occipital current density after training (i.e. increased inhibition of perceptual and visual G*f* components) and a decrease in the right inferior frontal gyrus (i.e. decreased inhibition of prefrontal inhibitory processes).

Overall, the present data reveal two potential correlates of fluid intelligence improvement in humans. First, a training-related increase of prefrontal cognitive control towards parietal regions, and second, a training-related decrease of inhibitory processes in visual areas specifically associated with a G*f* component requiring visuospatial processing. Further studies, possibly including multiple imaging techniques (e.g. fMRI and perfusion MRI), are warranted to verify such hypotheses and to test for the possible role of top-down modulation processes involving prefrontal and visual areas suggested by our data (Gazzaley et al. 2007). If replicated, these might be used to select targets for combined approaches including cognitive training and other modulatory techniques with known impact on brain

dynamics, such as neurofeedback (Sitaram et al. 2016; Zhang et al. 2015) and non-invasive brain stimulation (Santarnecchi et al. 2015a, b, c; Filmer et al. 2014).

Finally, the present findings also suggest the value of addressing the quest for the neurobiological basis of human intelligence by means of a confirmatory approach based on "cognitive perturbation", aimed at observing convergence of results going beyond the speculative nature of correlational studies (Santarnecchi and Rossi 2016b). In this regard, our cognitive training results support the idea of a distributed model underlying intelligence capacity (Jung and Haier 2007; Narr et al. 2007), with the changes in EEG dynamics accompanying successful training suggesting the importance of low-level—visual—computational processes, as well as prefrontal control over parietal dynamics.

Conclusions

Taken together, our findings support the notion that fast-changing, global neuroelectric patterns might be related to variability in G*f* levels in healthy humans. The degree of spontaneous activity of brain regions related to cognitive control and visual processing seems able to explain both variability in individual cognitive profiles and the response to a cognitive training exerting significant changes on individual G*f* scores. The present data also support the recent view about the nature of EEG microstates as being representative of inhibitory processes in the brain, offering a new insight about the link between human intelligence and spontaneous EEG activity.

Acknowledgements This research is based upon work supported by the Office of the Director of National Intelligence (ODNI), Intelligence Advanced Research Projects Activity (IARPA), via 2014-13121700007. The views and conclusions contained herein are those of the authors and should not be interpreted as necessarily representing the official policies or endorsements, either expressed or implied, of the ODNI, IARPA, or the U.S. Government. The U.S. Government is authorized to reproduce and distribute reprints for Governmental purposes notwithstanding any copyright annotation thereon. Dr. Pascual-Leone is further supported by the Berenson-Allen Foundation, the Sidney R. Baer Jr. Foundation, grants from the National Institutes of Health (R01HD069776, R01NS073601, R21 MH099196, R21 NS082870, R21 NS085491, R21 HD07616), and Harvard Catalyst | The Harvard Clinical and Translational Science Center (NCRR and the NCATS NIH, UL1 RR025758). The content of this paper is solely the responsibility of the authors and does not necessarily represent the official views of Harvard Catalyst, Harvard University and its affiliated academic health care centers, the National Institutes of Health, the Sidney R. Baer Jr. Foundation. The authors would like to thank the members of the larger Honeywell SHARP team for their valuable contributions to this work, including the SHARP Team authors: Harvard Medical School (Ann Connor, Franziska Plessow, Sadhvi Saxena, Erica Levenbaum); Honeywell (Jessamy Almquist, Michael Dillard, Umut Orhan, Santosh Mathan); Northeastern University (James McKanna, Deniz Erdogmus, Misha Pavel); Oxford University (Anna-Katharine Brem, Roi Cohen Kadosh, Nick Yeung); SimCoach Games (Garrett Kimball, Eben Myers).

References

Alexander GE, Furey ML, Grady CL, Pietrini P, Brady DR, Mentis MJ, Schapiro MB (1997) Association of premorbid intellectual function with cerebral metabolism in Alzheimer's disease: implications for the cognitive reserve hypothesis. Am J Psychiatry 154:165–172

Aron AR, Robbins TW, Poldrack RA (2014) Inhibition and the right inferior frontal cortex: one decade on. Trends Cogn Sci 18:177–185

Au J, Sheehan E, Tsai N, Duncan GJ, Buschkuehl M, Jaeggi SM (2014) Improving fluid intelligence with training on working memory: a meta-analysis. Psychon Bull Rev 22:366–377

Bartlett MS (1937) The statistical conception of mental factors. Br J Psychol 28:97–104

Beaujean AA, Firmin MW, Michonski JD, Berry T, Johnson C (2010) A multitrait–multimethod examination of the reynolds intellectual assessment scales in a college sample. Assessment 17:347–360

Benedek M, Jauk E, Sommer M, Arendasy M, Neubauer AC (2014) Intelligence, creativity, and cognitive control: the common and differential involvement of executive functions in intelligence and creativity. Intelligence 46:73–83

Bondarenko R, Boehler CN, Stoppel CM, Heinze HJ, Schoenfeld MA, Hopf JM (2012) Separable mechanisms underlying global feature-based attention. J Neurosci 32:15284–15295

Britz J, Van De Ville D, Michel CM (2010a) BOLD correlates of EEG topography reveal rapid resting-state network dynamics. Neuroimage 52:1162–1170

Britz J, Van De Ville D, Michel CM (2010b) BOLD correlates of EEG topography reveal rapid resting-state network dynamics. Neuroimage 52:1162–1170

Brumback CR, Low KA, Gratton G, Fabiani M (2004) Sensory ERPs predict differences in working memory span and fluid intelligence. Neuroreport 15:373–376

Brunet D, Murray MM, Michel CM (2011) Spatiotemporal analysis of multichannel EEG: CARTOOL. Comput Intell Neurosci 2011:813870

Burgess GC, Gray JR, Conway AR, Braver TS (2011) Neural mechanisms of interference control underlie the relationship between fluid intelligence and working memory span. J Exp Psychol Gen 140:674–692

Buschman TJ, Siegel M, Roy JE, Miller EK (2011) Neural substrates of cognitive capacity limitations. Proc Natl Acad Sci USA 108:11252–11255

Carpenter PA, Just MA, Shell P (1990) What one intelligence test measures: a theoretical account of the processing in the Raven Progressive Matrices Test. Psychol Rev 97:404–431

Chiang MC, Barysheva M, Lee AD, Madsen S, Klunder AD, Toga AW, McMahon KL, de Zubicaray GI, Meredith M, Wright MJ, Srivastava A, Balov N, Thompson PM (2008) Brain fiber architecture, genetics, and intelligence: a high angular resolution diffusion imaging (HARDI) study. Med Image Comput Comput Assist Interv 11:1060–1067

Choi YY, Shamosh NA, Cho SH, Deyoung CG, Lee MJ, Lee JM, Kim SI, Cho ZH, Kim K, Gray JR, Lee KH (2008) Multiple bases of human intelligence revealed by cortical thickness and neural activation. J Neurosci 28:10323–10329

Cole JC, Lopez BR, Daleo DV (2004) Latent relationships of fluid, visual, and simultaneous cognitive tasks. Psychol Rep 94:547–561

Cole MW, Yarkoni T, Repovs G, Anticevic A, Braver TS (2012) Global connectivity of prefrontal cortex predicts cognitive control and intelligence. J Neurosci 32:8988–8999

Colom R, Jung RE, Haier RJ (2006) Distributed brain sites for the g-factor of intelligence. Neuroimage 31:1359–1365

Colom R, Karama S, Jung RE, Haier RJ (2010) Human intelligence and brain networks. Dialogues Clin Neurosci 12:489–501

Colom R, Burgaleta M, Roman FJ, Karama S, Alvarez-Linera J, Abad FJ, Martinez K, Quiroga MA, Haier RJ (2013) Neuroanatomic overlap between intelligence and cognitive factors: morphometry methods provide support for the key role of the frontal lobes. Neuroimage 72:143–152

Crone EA, Wendelken C, van LL, Honomichl RD, Christoff K, Bunge SA (2009) Neurocognitive development of relational reasoning. Dev Sci 12:55–66

da Rocha AF, Rocha FT, Massad E (2011) The brain as a distributed intelligent processing system: an EEG study. PLoS ONE 6:e17355

Damoiseaux JS, Rombouts SA, Barkhof F, Scheltens P, Stam CJ, Smith SM, Beckmann CF (2006) Consistent resting-state networks across healthy subjects. Proc Natl Acad Sci USA 103:13848–13853

Dang CP, Braeken J, Colom R, Ferrer E, Liu C (2014) Why is working memory related to intelligence? Different contributions from storage and processing. Memory 22:426–441

Deary I (2008) Why do intelligent people live longer? Nature 456:175–176

Deary IJ, Penke L, Johnson W (2010) The neuroscience of human intelligence differences. Nat Rev Neurosci 11:201–211

Delorme A, Makeig S (2004) EEGLAB: an open source toolbox for analysis of single-trial EEG dynamics including independent component analysis. J Neurosci Methods 134:9–21

Engle RW, Tuholski SW, Laughlin JE, Conway AR (1999) Working memory, short-term memory, and general fluid intelligence: a latent-variable approach. J Exp Psychol Gen 128:309–331

Filmer HL, Dux PE, Mattingley JB (2014) Applications of transcranial direct current stimulation for understanding brain function. Trends Neurosci 37:742–753

Gaspar JM, McDonald JJ (2014) Suppression of salient objects prevents distraction in visual search. J Neurosci 34:5658–5666

Gazzaley A, Cooney JW, Rissman J, D'Esposito M (2005) Top-down suppression deficit underlies working memory impairment in normal aging. Nat Neurosci 8:1298–1300

Gazzaley A, Rissman J, Cooney J, Rutman A, Seibert T, Clapp W, D'Esposito M (2007) Functional interactions between prefrontal and visual association cortex contribute to top-down modulation of visual processing. Cereb Cortex 17(Suppl 1):i125–i135

Goh S, Bansal R, Xu D, Hao X, Liu J, Peterson BS (2011) Neuroanatomical correlates of intellectual ability across the life span. Dev Cogn Neurosci 1:305–312

Gong QY, Sluming V, Mayes A, Keller S, Barrick T, Cezayirli E, Roberts N (2005) Voxel-based morphometry and stereology provide convergent evidence of the importance of medial prefrontal cortex for fluid intelligence in healthy adults. Neuroimage 25:1175–1186

Gray JR, Thompson PM (2004a) Neurobiology of intelligence: health implications? Discov Med 4:157–162

Gray JR, Thompson PM (2004b) Neurobiology of intelligence: science and ethics. Nat Rev Neurosci 5:471–482

Gray JR, Chabris CF, Braver TS (2003) Neural mechanisms of general fluid intelligence. Nat Neurosci 6:316–322

Haier RJ (2014) Increased intelligence is a myth (so far). Front Syst Neurosci 8:34

Haier RJ, Jung RE, Yeo RA, Head K, Alkire MT (2004) Structural brain variation and general intelligence. Neuroimage 23:425–433

Hambrick DZ, Altmann EM (2015) The role of placekeeping ability in fluid intelligence. Psychon Bull Rev 22:1104–1110

Hossiep R, Turck D, Hasella M (1999) Bochumer Matrizentest: BOMAT advanced-short version. Hogrefe, Göttingen

Houde O, Zago L, Mellet E, Moutier S, Pineau A, Mazoyer B, Tzourio-Mazoyer N (2000) Shifting from the perceptual brain to the logical brain: the neural impact of cognitive inhibition training. J Cogn Neurosci 12:721–728

Jacob SN, Nieder A (2014) Complementary roles for primate frontal and parietal cortex in guarding working memory from distractor stimuli. Neuron 83:226–237

Jaeggi SM, Buschkuehl M, Jonides J, Perrig WJ (2008) Improving fluid intelligence with training on working memory. Proc Natl Acad Sci USA 105:6829–6833

Jung RE, Haier RJ (2007) The Parieto-Frontal Integration Theory (P-FIT) of intelligence: converging neuroimaging evidence. Behav Brain Sci 30:135–154

Kaiser FH (1958) The varimax criterion for analytic rotation in factor analysis. Psychometrika 23:187–200

Khanna A, Pascual-Leone A, Farzan F (2014) Reliability of resting-state microstate features in electroencephalography. PLoS ONE 9:e114163

Khanna A, Pascual-Leone A, Michel CM, Farzan F (2015) Microstates in resting-state EEG: current status and future directions. Neurosci Biobehav Rev 49:105–113

Kievit RA, Davis SW, Mitchell DJ, Taylor JR, Duncan J, Henson RN (2014) Distinct aspects of frontal lobe structure mediate age-related differences in fluid intelligence and multitasking. Nat Commun 5:5658

Koenig T, Lehmann D (1996) Microstates in language-related brain potential maps show noun-verb differences. Brain Lang 53:169–182

Koenig T, Melie-Garcia L (2009) Statistical analysis of multichannel scalp field data. In: Koenig T, Melie-Garcia L, Electrical neuroimaging. Cambridge University, Cambridge 53:169–190

Koenig T, Kochi K, Lehmann D,(1998) Event-related electric microstates of the brain differ between words with visual and abstract meaning. Electroencephalogr Clin Neurophysiol 106:535–546

Koenig T, Prichep L, Lehmann D, Sosa PV, Braeker E, Kleinlogel H, Isenhart R, John ER (2002) Millisecond by millisecond, year by year: normative EEG microstates and developmental stages. Neuroimage 16:41–48

Kundu B, Sutterer DW, Emrich SM, Postle BR (2013) Strengthened effective connectivity underlies transfer of working memory training to tests of short-term memory and attention. J Neurosci 33:8705–8715

Kush JC, Spring MB, Barkand J (2012) Advances in the assessment of cognitive skills using computer-based measurement. Behav Res Methods 44:125–134

Lancaster JL, Woldorff MG, Parsons LM, Liotti M, Freitas CS, Rainey L, Kochunov PV, Nickerson D, Mikiten SA, Fox PT (2000) Automated Talairach atlas labels for functional brain mapping. Hum Brain Mapp 10(3):120–131

Langer N, von Bastian CC, Wirz H, Oberauer K, Jancke L (2013) The effects of working memory training on functional brain network efficiency. Cortex 49:2424–2438

Lehmann D (1971) Multichannel topography of human alpha EEG fields. Electroencephalogr Clin Neurophysiol 31:439–449

Lehmann D, Faber PL, Galderisi S, Herrmann WM, Kinoshita T, Koukkou M, Mucci A, Pascual-Marqui RD, Saito N, Wackermann J, Winterer G, Koenig T (2005) EEG microstate duration and syntax in acute, medication-naive, first-episode schizophrenia: a multi-center study. Psychiatry Res 138:141–156

Malhotra P, Coulthard EJ, Husain M (2009) Role of right posterior parietal cortex in maintaining attention to spatial locations over time. Brain 132:645–660

Martinez A, Anllo-Vento L, Sereno MI, Frank LR, Buxton RB, Dubowitz DJ, Wong EC, Hinrichs H, Heinze HJ, Hillyard SA (1999) Involvement of striate and extrastriate visual cortical areas in spatial attention. Nat Neurosci 2:364–369

Matsuda O, Saito M (1998) Crystallized and fluid intelligence in elderly patients with mild dementia of the Alzheimer type. Int Psychogeriatr 10:147–154

Matzen LE, Benz ZO, Dixon KR, Posey J, Kroger JK, Speed AE (2010) Recreating Raven's: software for systematically generating large numbers of Raven-like matrix problems with normed properties. Behav Res Methods 42:525–541

Mazziotta J, Toga A, Evans A, Fox P, Lancaster J, Zilles K et al (2001) A four-dimensional probabilistic atlas of the human brain. J Am Med Inf Assoc, 8(5):401–430

Melara RD, Tong Y, Rao A (2012) Control of working memory: effects of attention training on target recognition and distractor salience in an auditory selection task. Brain Res 1430:68–77

Melnick MD, Harrison BR, Park S, Bennetto L, Tadin D (2013) A strong interactive link between sensory discriminations and intelligence. Curr Biol 23:1013–1017

Michel CM, Lehmann D (1993) Single doses of piracetam affect 42-channel event-related potential microstate maps in a cognitive paradigm. Neuropsychobiology 28:212–221

Micheloyannis S, Pachou E, Stam CJ, Vourkas M, Erimaki S, Tsirka V (2006) Using graph theoretical analysis of multi channel EEG to evaluate the neural efficiency hypothesis. Neurosci Lett 402:273–277

Milz P, Faber PL, Lehmann D, Koenig T, Kochi K, Pascual-Marqui RD (2015) The functional significance of EEG microstates-associations with modalities of thinking. Neuroimage 125:643–656

Mognon A, Jovicich J, Bruzzone L, Buiatti M (2011) ADJUST: an automatic EEG artifact detector based on the joint use of spatial and temporal features. Psychophysiology 48:229–240

Moody S (2009) Can intelligence be increased by training on a task of working memory? Intelligence 7:327–328

Narr KL, Woods RP, Thompson PM, Szeszko P, Robinson D, Dimtcheva T, Gurbani M, Toga AW, Bilder RM (2007) Relationships between IQ and regional cortical gray matter thickness in healthy adults. Cereb Cortex 17:2163–2171

Neubauer AC, Fink A (2009) Intelligence and neural efficiency. Neurosci Biobehav Rev 33:1004–1023

Neubauer AC, Grabner RH, Freudenthaler HH, Beckmann JF, Guthke J (2004) Intelligence and individual differences in becoming neurally efficient. Acta Psychol 116:55–74

Nichols TE, Holmes AP (2002) Nonparametric permutation tests for functional neuroimaging: a primer with examples. Hum Brain Mapp 15(1):1–25

Nishida K, Morishima Y, Yoshimura M, Isotani T, Irisawa S, Jann K, Dierks T, Strik W, Kinoshita T, Koenig T (2013) EEG microstates associated with salience and frontoparietal networks in frontotemporal dementia, schizophrenia and Alzheimer's disease. Clin Neurophysiol 124(6):1106–1114

Oelhafen S, Nikolaidis A, Padovani T, Blaser D, Koenig T, Perrig WJ (2013) Increased parietal activity after training of interference control. Neuropsychologia 51:2781–2790

Pahor A, Jausovec N (2014) The effects of theta transcranial alternating current stimulation (tACS) on fluid intelligence. Int J Psychophysiol 93:322–331

Pascual-Marqui RD (2007) Discrete, 3D distributed, linear imaging methods of electric neuronal activity. Part 1: exact, zero error localization. arXiv:0710.3341 [Math-Ph, Physics:physics, Q-Bio], October

Pascual-Marqui RD, Michel CM, Lehmann D (1995) Segmentation of brain electrical activity into microstates: model estimation and validation. IEEE Trans Biomed Eng 42:658–665

Pascual-Marqui RD, Lehmann D, Faber P, Milz P, Kochi K, Yoshimura M, Nishida K, Isotani T, Kinoshita T (2014) The resting microstate networks (RMN): cortical distributions, dynamics, and frequency specific information flow. http://arxiv.org/abs/1411.1949v2

Pereira J, Wang XJ (2015) A tradeoff between accuracy and flexibility in a working memory circuit endowed with slow feedback mechanisms. Cereb Cortex 25:3586–3601

Perfetti B, Saggino A, Ferretti A, Caulo M, Romani GL, Onofrj M (2009) Differential patterns of cortical activation as a function of fluid reasoning complexity. Hum Brain Mapp 30:497–510

Peters JC, Roelfsema PR, Goebel R (2012) Task-relevant and accessory items in working memory have opposite effects on activity in extrastriate cortex. J Neurosci 32:17003–17011

Prado J, Noveck IA (2007) Overcoming perceptual features in logical reasoning: a parametric functional magnetic resonance imaging study. J Cogn Neurosci 19:642–657

Prado J, Kaliuzhna M, Cheylus A, Noveck IA (2008) Overcoming perceptual features in logical reasoning: an event-related potentials study. Neuropsychologia 46:2629–2637

Prado J, Van Der Henst JB, Noveck IA (2010) Recomposing a fragmented literature: how conditional and relational arguments engage different neural systems for deductive reasoning. Neuroimage 51:1213–1221

Raven J, Raven JC, Court JH (2003) Manual for Raven's progressive matrices and vocabulary scales. Section 1: general overview. Harcourt Assessment, San Antonia

Raz N, Lindenberger U, Ghisletta P, Rodrigue KM, Kennedy KM, Acker JD (2008) Neuroanatomical correlates of fluid intelligence in healthy adults and persons with vascular risk factors. Cereb Cortex 18:718–726

Rushton JP, Ankney CD (2009) Whole brain size and general mental ability: a review. Int J Neurosci 119:691–731

Santarnecchi E, Rossi S (2016b) Advances in the neuroscience of intelligence: from brain connectivity to brain perturbation. Span J Psychol. doi:10.1017/sjp.2016.89

Santarnecchi E, Polizzotto NR, Godone M, Giovannelli F, Feurra M, Matzen L, Rossi A, Rossi S (2013) Frequency-dependent enhancement of fluid intelligence induced by transcranial oscillatory potentials. Curr Biol 23:1449–1453

Santarnecchi E, Galli G, Polizzotto NR, Rossi A, Rossi S (2014) Efficiency of weak brain connections support general cognitive functioning. Hum Brain Mapp 35:4566–4582

Santarnecchi E, Brem AK, Levenbaum E, Thompson T, Kadosh RC, Pascual-Leone A (2015a) Enhancing cognition using transcranial electrical stimulation. Curr Opin Behav Sci 4:171–178

Santarnecchi E, Rossi S, Rossi A (2015b) The smarter, the stronger: intelligence level correlates with brain resilience to systematic insults. Cortex 64:293–309

Santarnecchi E, Tatti E, Rossi S, Serino V, Rossi A (2015c) Intelligence-related differences in the asymmetry of spontaneous cerebral activity. Hum Brain Mapp 36:3586–3602

Santarnecchi E, Muller T, Rossi S, Sarkar A, Polizzotto NR, Rossi A, Kadosh RC (2016a) Individual differences and specificity of prefrontal gamma frequency-tACS on fluid intelligence capabilities. Cortex 23:1449–1453

Sitaram R, Ros T, Stoeckel L, Haller S, Scharnowski F, Lewis-Peacock J, Weiskopf N et al (2016) Closed-loop brain training: the science of neurofeedback. Nat Rev Neurosci 18(2):86–100

Soulieres I, Dawson M, Samson F, Barbeau EB, Sahyoun CP, Strangman GE, Zeffiro TA, Mottron L (2009) Enhanced visual processing contributes to matrix reasoning in autism. Hum Brain Mapp 30:4082–4107

Stern Y (2002) What is cognitive reserve? Theory and research application of the reserve concept. J Int Neuropsychol Soc 8:448–460

Stern Y (2009) Cognitive reserve. Neuropsychologia 47:2015–2028
Thompson TW, Waskom ML, Garel KL, Cardenas-Iniguez C, Reynolds GO, Winter R, Chang P, Pollard K, Lala N, Alvarez GA, Gabrieli JD (2013) Failure of working memory training to enhance cognition or intelligence. PLoS ONE 8:e63614
Tibshirania R, Walther G (2005) Cluster validation by prediction strength. J Comput Graph Stat 14:511–528
Tomescu MI, Rihs TA, Becker R, Britz J, Custo A, Grouiller F, Schneider M, Debbane M, Eliez S, Michel CM (2014) Deviant dynamics of EEG resting state pattern in 22q11.2 deletion syndrome adolescents: a vulnerability marker of schizophrenia? Schizophr Res 157:175–181
Vakhtin AA, Ryman SG, Flores RA, Jung RE (2014) Functional brain networks contributing to the Parieto-Frontal Integration Theory of Intelligence. Neuroimage 103:349–354
Van De Ville D, Britz J, Michel CM (2010) EEG microstate sequences in healthy humans at rest reveal scale-free dynamics. Proc Natl Acad Sci USA 107:18179–18184
van den Heuvel MP, Stam CJ, Kahn RS, Hulshoff Pol HE (2009) Efficiency of functional brain networks and intellectual performance. J Neurosci 29:7619–7624
Verney SP, Granholm E, Marshall SP, Malcarne VL, Saccuzzo DP (2005) Culture-fair cognitive ability assessment: information processing and psychophysiological approaches. Assessment 12:303–319
Wartenburger I, Heekeren HR, Preusse F, Kramer J, van der Meer E (2009) Cerebral correlates of analogical processing and their modulation by training. Neuroimage 48:291–302
Whalley LJ, Deary IJ, Appleton CL, Starr JM (2004) Cognitive reserve and the neurobiology of cognitive aging. Ageing Res Rev 3:369–382
Yuan Z, Qin W, Wang D, Jiang T, Zhang Y, Yu C (2012) The salience network contributes to an individual's fluid reasoning capacity. Behav Brain Res 229:384–390
Zhang G, Yao L, Shen J, Yang Y, Zhao X (2015) Reorganization of functional brain networks mediates the improvement of cognitive performance following real-time neurofeedback training of working memory: brain networks mediate post-training behavior. Hum Brain Mapp 36(5):1705–1715
Zook NA, Davalos DB, Delosh EL, Davis HP (2004) Working memory, inhibition, and fluid intelligence as predictors of performance on Tower of Hanoi and London tasks. Brain Cogn 56:286–292